Collective-model description of shape coexistence and intruder states in cadmium isotopes based on a relativistic energy density functional

K. Nomura [1,*] and K. E. Karakatsanis [1,2]

[1]*Department of Physics, Faculty of Science, University of Zagreb, HR-10000 Zagreb, Croatia*

[2]*Physics Department, Aristotle University of Thessaloniki, Thessaloniki GR-54124, Greece*

(Received 20 September 2022; accepted 1 December 2022; published 15 December 2022)

Low-energy structure of even-even $^{108-116}$Cd isotopes is analyzed using a collective model that is based on the nuclear density functional theory. Spectroscopic properties are computed by solving the triaxial quadrupole collective Hamiltonian, with parameters determined by the constrained self-consistent mean-field calculations within the relativistic Hartree-Bogoliubov method employing a universal energy density functional and a pairing force. The collective Hamiltonian reproduces the observed quadrupole phonon states of vibrational character, which are based on the moderately deformed equilibrium minimum in the mean-field potential energy surface. In addition, the calculation yields a low-lying excited 0^+ band and a γ-vibrational band that are associated with a deformed local minimum close in energy to the ground state, consistently with the empirical interpretation of these bands as intruder bands. Observed energy spectra, $B(E2)$, and $\rho^2(E0)$ values are, in general, reproduced reasonably well.

DOI: 10.1103/PhysRevC.106.064317

I. INTRODUCTION

Quadrupole collectivity is a basic, yet prominent, feature of nuclear structure, characterized by the (anharmonic) vibrations of a spherical nuclear surface or the rotations of an ellipsoidal deformed nuclear shape [1–4]. A collective vibrational spectrum is, in particular, observed in nearly spherical nuclei, and is interpreted in terms of the excitations of quadrupole phonons. The energy spectrum then consists of zero- (0^+) and one-phonon (2^+) states, followed by a two-phonon triplet (4^+, 2^+, 0^+) at twice the excitation energy of the one-phonon state, and so on. Classic examples of the vibrational energy spectrum have been known in stable nuclei near the proton $Z = 50$ magic number, such as the even-even cadmium (Cd) [5], where the observed low-lying states indeed show features that resemble the quadrupole vibrational spectra predicted by the collective model of Bohr and Mottelson [1].

Later experiments have revealed, however, in addition to the multiphonon states, extra 0^+ and 2^+ levels that are close in energy to the two-phonon triplet in even-even Cd [6]. The appearance of these additional states is not explained in a vibrational picture, but rather implies that the pure quadrupole phonon interpretation of even-even Cd is untenable. In a spherical shell model the additional states were attributed to two-particle–two-hole (2p-2h) excitations of protons from above the $Z = 50$ shell gap. Correlations between the valence protons and neutrons can be then so enhanced that the lowering of the intruder low-spin levels occurs [7–12]. The interpretation of the extra 0^+ and 2^+ states in Cd as 2p-4h states was confirmed by the (^{3}He, n) reaction experiment [13].

Furthermore, in the mean-field approximation [10,12,14–16] the normal and intruder states correspond to different minima on the potential energy surface defined in terms of the quadrupole deformations.

Along the chain of even-even Cd isotopes, the intruder bands have been shown to become lower in energy toward the middle of the major shell $N = 66$ with the increasing number of valence neutrons. The structure of the even-even Cd has been studied by numerous experiments, most extensively, on stable isotopes with the mass $A = 106$ to $A = 116$. An extensive list of the references to the related experimental studies is found in Ref. [17]. Recent reviews on the experimental and theoretical studies on the structure of the light and heavy Cd isotopes, as well as the neighboring isotopes in the tin (Sn) region, are given in Refs. [12,18–20].

Besides that, theoretical investigations of the even-even Cd have been performed from various perspectives. Large-scale shell model calculations have been carried out from the light ($A \approx 98$) [21–23] up to the mass $A = 108$ [24] Cd. As a more plausible approach that represents a drastic truncation of the shell model configuration space, calculations within an extended version of the interacting boson model (IBM) [4] that takes into account the 2p-2h intruder excitations and configuration mixing between the normal (0p-0h) and intruder states have been carried out extensively [9,11,17,25–32]. Alternative approaches are self-consistent mean-field (SCMF) methods [2] based on the nuclear density functional theory (DFT). Calculations within the symmetry-projected SCMF method using the Gogny-type [33,34] energy density functional (EDF) were performed to analyze the systematic behavior of the 2_1^+ state of the even-even Cd in the entire $N = 50$–82 major shell [35], to provide detailed descriptions of the spectroscopy of the ^{110,112}Cd nuclei [36,37], and to describe in a systematic

*knomura@phy.hr

manner the low-energy structure of the even-even $^{98-130}$Cd nuclei in comparison with the updated experimental data [38]. A quadrupole collective Bohr Hamiltonian, derived from a microscopic framework of the adiabatic time-dependent Hartree-Fock-Bogoliubov method using a Skyrme force [39], was considered for $^{110-116}$Cd [40].

Here we present an alternative theoretical description of the even-even $^{108-116}$Cd nuclei using the triaxial quadrupole collective Hamiltonian (QCH) that is based on the nuclear DFT. Within this theoretical scheme, parameters of the QCH are determined by using as microscopic inputs the solutions of the SCMF calculations based on a universal EDF and a pairing interaction. We shall identify, in most of the studied nuclei, low-energy collective bands that are associated with intruder bands as empirically suggested, and discuss their microscopic structures in connection with shape coexistence. In Sec. II, we give a brief description of the SCMF and QCH approaches. Results of the SCMF calculations are shown in Sec. III. In Sec. IV, we present the QCH results of the spectroscopic calculations, including the excitation energies, electric quadrupole and monopole transition rates, and detailed spectroscopy of ^{110,112}Cd. Finally, Sec. V gives a summary of the main results.

II. THEORETICAL FRAMEWORK

The first step in the theoretical procedure is to perform, for each nucleus, a set of the constrained SCMF calculations within the framework of the relativistic Hartree-Bogoliubov (RHB) method [41–44] employing the density-dependent point-coupling (DD-PC1) interaction [45] and the separable pairing force of finite range developed in [46]. The constraints imposed in the SCMF calculations are on the expectation values of the mass quadrupole operators

$$\hat{Q}_{20} = 2z^2 - x^2 - y^2 \quad \text{and} \quad \hat{Q}_{22} = x^2 - y^2, \tag{1}$$

which are related to the axially symmetric deformation β and triaxiality γ [1], i.e.,

$$\beta = \sqrt{\frac{5}{16\pi}}\frac{4\pi}{3}\frac{1}{A(r_0A^{1/3})^2}\sqrt{\langle\hat{Q}_{20}\rangle^2 + 2\langle\hat{Q}_{22}\rangle^2}, \tag{2}$$

$$\gamma = \arctan\sqrt{2}\frac{\langle\hat{Q}_{22}\rangle}{\langle\hat{Q}_{20}\rangle}, \tag{3}$$

with $r_0 = 1.2$ fm. The SCMF calculations are carried out in a harmonic oscillator basis, with the number of oscillator shells equal to 20. The strengths of the proton V_p and neutron V_n pairings are set equal, $V_0 \equiv V_p = V_n = 728$ MeV fm^3, which have been obtained in Ref. [46] so that the pairing gaps provided by the Gogny-D1S [34] SCMF calculation are reproduced.

Quadrupole collective states are obtained as the solutions to the QCH. The parameters of the Hamiltonian are specified by using the results of the RHB calculations: the potential energy surfaces as functions of the β and γ deformations, and the single-particle solutions. The detailed accounts of this procedure are found in Refs. [42,47]. The collective Hamiltonian $\hat{H}_{\rm coll}$ is given as

$$\hat{H}_{\rm coll} = \hat{T}_{\rm vib} + \hat{T}_{\rm rot} + V_{\rm coll}, \tag{4}$$

with the vibrational kinetic energy

$$\hat{T}_{\rm vib} = -\frac{\hbar^2}{2\sqrt{wr}}\left[\frac{1}{\beta^4}\left(\frac{\partial}{\partial\beta}\sqrt{\frac{r}{w}}\beta^4 B_{\gamma\gamma}\frac{\partial}{\partial\beta} - \frac{\partial}{\partial\beta}\sqrt{\frac{r}{w}}\beta^3 B_{\beta\gamma}\frac{\partial}{\partial\gamma}\right)\right.$$
$$\left. + \frac{1}{\beta\sin 3\gamma}\left(-\frac{\partial}{\partial\gamma}\sqrt{\frac{r}{w}}\sin 3\gamma B_{\beta\gamma}\frac{\partial}{\partial\beta} + \frac{1}{\beta}\frac{\partial}{\partial\gamma}\sqrt{\frac{r}{w}}\sin 3\gamma B_{\beta\beta}\frac{\partial}{\partial\gamma}\right)\right], \tag{5}$$

rotational kinetic energy

$$\hat{T}_{\rm rot} = \frac{1}{2}\sum_{k=1}^{3}\frac{\hat{J}_k^2}{\mathcal{I}_k}, \tag{6}$$

and collective potential $V_{\rm coll}$. Note the operator $\hat{J}_k$ in Eq. (6) denotes the components of the angular momentum in the body-fixed frame of a nucleus. The mass parameters $B_{\beta\beta}$, $B_{\beta\gamma}$, and $B_{\gamma\gamma}$ in (5), and the moments of inertia $\mathcal{I}_k$ in (6), are functions of the β and γ deformations, and are related to each other by $\mathcal{I}_k = 4B_k\beta^2\sin^2(\gamma - 2k\pi/3)$. Two additional quantities in Eq. (5), i.e., $r = B_1B_2B_3$ and $w = B_{\beta\beta}B_{\gamma\gamma} - B_{\beta\gamma}^2$, determine the volume element in the collective space. The moments of inertia are computed using the Inglis-Belyaev formula [48,49], and the mass parameters are calculated in the cranking approximation. The collective potential $V_{\rm coll}$ (4) is obtained by subtracting the zero-point energy corrections from the total RHB deformation energy.

The corresponding eigenvalue problem is solved using an expansion of eigenfunctions in terms of a complete set of basis functions that depend on the deformation variables β and γ, and the Euler angles $\Omega = (\phi, \theta, \psi)$. The diagonalization of the Hamiltonian yields the excitation energies and collective wave functions for each value of the total angular momentum and parity, that are used to calculate various physical observables. A virtue of using the QCH based on SCMF single-(quasi)particle solutions is the fact that the observables, such as electric quadrupole ($E2$) and monopole ($E0$) transition probabilities and spectroscopic quadrupole moments, are calculated in the full configuration space and there is no need for effective charges. Using the bare value of the proton charge in the electric transition operators, the transition probabilities between eigenvectors of the QCH can be directly compared with spectroscopic data.

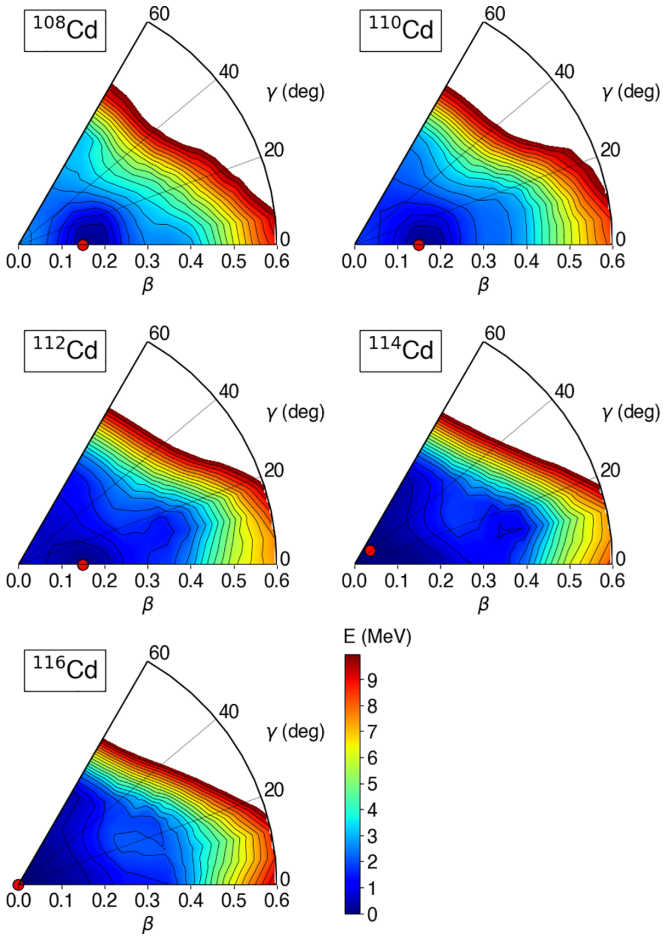

FIG. 1. Potential energy surfaces for the even-even $^{108-116}$Cd nuclei as functions of the triaxial quadrupole β-γ deformations, computed by the constrained SCMF calculations within the RHB framework employing the interaction DD-PC1 and the separable pairing force of finite range. The total SCMF energies are plotted up to 10 MeV from the global minimum (indicated by the solid circle), and the energy difference between neighboring contours is 0.5 MeV.

III. MEAN-FIELD RESULTS

Figure 1 shows the β-γ triaxial potential energy surfaces for $^{108-116}$Cd calculated by using the constrained RHB method. The global minimum occurs at a weakly deformed prolate configuration $\beta \approx 0.15$ for ^{108,110,112}Cd, and at a nearly spherical configuration for ^{114,116}Cd. Besides the weakly deformed global minimum, in most of the nuclei two local minima with larger deformation $\beta \gtrsim 0.3$ are obtained on both prolate ($\gamma = 0^\circ$) and oblate ($\gamma = 60^\circ$) sides. In particular, a pronounced triaxial local minimum near the prolate axis, $(\beta, \gamma) \approx (0.35, 12^\circ)$, which is close in energy to the global minimum, is suggested to occur for ^{112,114}Cd.

The appearance of the minima in the potential energy surface is inferred from the behaviors of the single-particle levels near the Fermi energies. Figure 2 shows the single-particle energies for protons and neutrons for ^{112}Cd as functions of the axial quadrupole deformation β, obtained as the SCMF solutions. In the proton single-particle spectra, near the Fermi energy (indicated by a dash-dotted curve in Fig. 2), there is a gap within the range $0.05 \lesssim \beta \lesssim 0.3$. The gap is produced essentially by the $g_{9/2}$ and $g_{7/2}$ orbitals, coming respectively from below and above the $Z = 50$ major shell. In this range of deformation the global prolate minimum is obtained in the potential energy surface (see Fig. 1). Another gap is seen in the single-proton spectra at $\beta \approx 0.35$, which is produced by the $g_{9/2}$ and $p_{1/2}$ from below the $Z = 50$ major shell, and $g_{7/2}$ and $d_{5/2}$ from above. This corresponds to the local minimum that appears near the prolate axis $(\beta, \gamma) \approx (0.35, 12^\circ)$. On the oblate side ($\beta < 0$), yet another gap is visible in the interval $-0.4 \lesssim \beta \lesssim -0.2$, created as a result of the lowering of the $g_{7/2}$ levels and the rising of the $g_{9/2}$, $p_{1/2}$, and $p_{3/2}$ ones. The gap is related to the oblate local minimum. The fact that the several energy gaps are obtained in the proton single-particle diagram conforms to the empirical interpretation that the observed extra low-spin states in Cd isotopes are attributed to particle-hole excitations of protons across the $Z = 50$ closed shell. Similarly, one could see in the neutron single-particle spectra (shown on the right-hand side of Fig. 2) energy gaps near the Fermi energy in those same ranges of the β deformation at which the local minima occur in the potential energy surface. The gaps are, however, much less pronounced, i.e., the level density around the Fermi surface is much higher, than in the case of the single-proton spectra. It should be noted that the above argument, in terms of the appearance of the minima in the potential energy surface and the gaps in the single-particle levels, is made at the mean-field level, and provides only an approximate picture of low-lying states.

We further study the sensitivity of the calculations to the strengths of the proton V_p and neutron V_n pairing interactions. As an example, we show in Fig. 3 the potential energy surfaces for ^{112}Cd computed with the pairing strengths unchanged, i.e., $V_p = V_n = 728$ MeV fm^3 ($= V_0$), and increased by 15% for both protons and neutrons, i.e., $V_p = V_n = 1.15V_0 = 837$ MeV fm^3. A comparison between the two surfaces in Fig. 3 shows that, with the increased pairing strength, the global minimum shifts to the spherical side, $\beta \approx 0.05$, while the triaxial local minimum becomes much less pronounced. The same conclusion was reached in [17] where the constrained Hartree-Fock plus BCS calculations for ^{112}Cd using the Skyrme SLy6 force [50] were employed as the input to build the IBM Hamiltonian with configuration mixing. In the following, we mainly discuss results with the original pairing strength in the RHB calculations ($V_p = V_n = V_0$), while the dependence of the spectroscopic properties on the pairing strengths will also be analyzed.

IV. SPECTROSCOPIC RESULTS

Figure 4 shows the calculated low-energy excitation spectra, $B(E2; 0_2^+ \to 2_1^+)$ and $\rho^2(E0; 0_2^+ \to 0_1^+)$ transition probabilities for the even-even nuclei $^{108-116}$Cd. Experimental data are taken from Refs. [19,36,37,51,52]. For $^{108-114}$Cd, the 0_2^+ state has been empirically suggested to be the bandhead of the intruder band associated with the proton 2p-2h excitations [53]. As for ^{116}Cd, the 0_3^+ state has been identified as the lowest intruder state. For all five nuclei, the 2_3^+ state is attributed

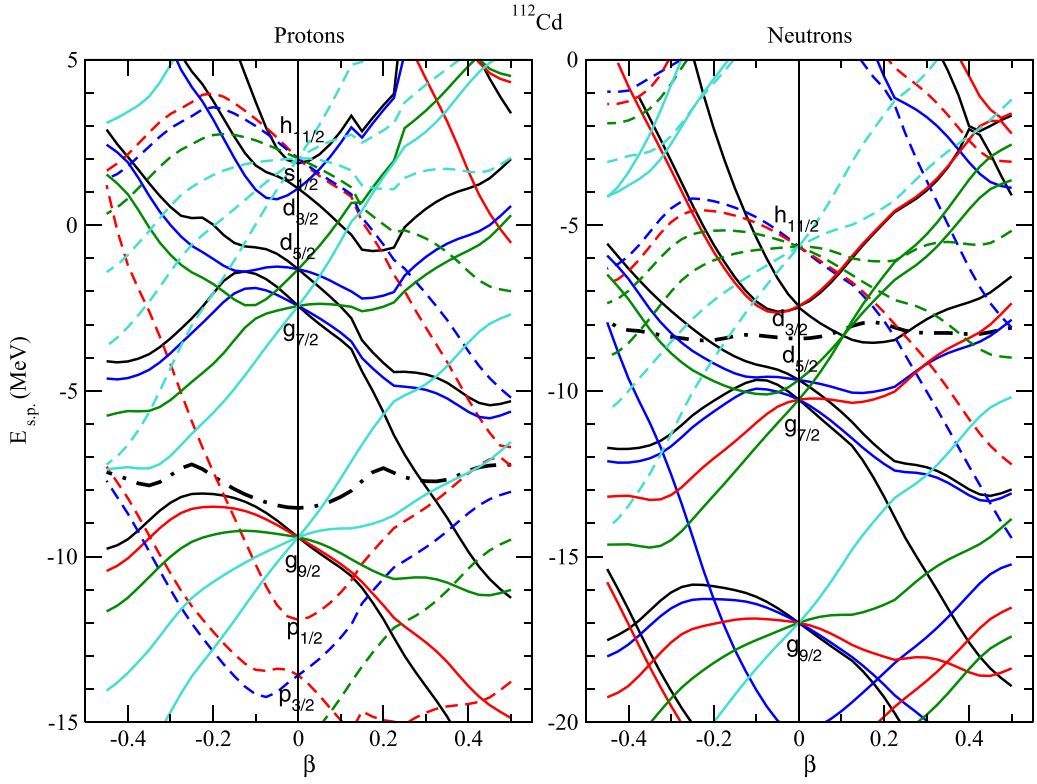

FIG. 2. Calculated single-particle energies for protons (left) and neutrons (right) for ^{112}Cd as functions of the axial quadrupole deformation β. Dash-dotted curves represent Fermi energies.

to the first excited state of the intruder band by experiments. In the present RHB+QCH calculation, as shown later, the 0_2^+ and 2_2^+ states are considered as the corresponding intruder states. Only for ^{108}Cd, the 2_3^+ state is here suggested to be of intruder nature.

The present calculation reproduces the energies of the normal, i.e., phonon-like, states (2_1^+, 4_1^+, 6_1^+, 3_1^+, 2_2^+, and 0_3^+) fairly well. The observed intruder 0^+ and 2^+ states gradually decrease in energy and become lowest at ^{114}Cd corresponding to the midshell $N = 66$. The measured $E2$ and $E0$ transitions from the intruder $0^+_{\rm intr}$ state, i.e., $B(E2; 0^+_{\rm intr} \to 2_1^+)$ and $\rho^2(E0; 0^+_{\rm intr} \to 0_1^+)$, also increase toward ^{114}Cd. The RHB+QCH calculation gives similar systematic behaviors of these quantities, but underestimates the intruder 0^+ and 2^+ level energies for ^{112,114}Cd significantly. Moreover, the predicted $B(E2; 0_2^+ \to 2_1^+)$ and $\rho^2(E0; 0_2^+ \to 0_1^+)$ values are generally a factor of two to three larger than the experimental values.

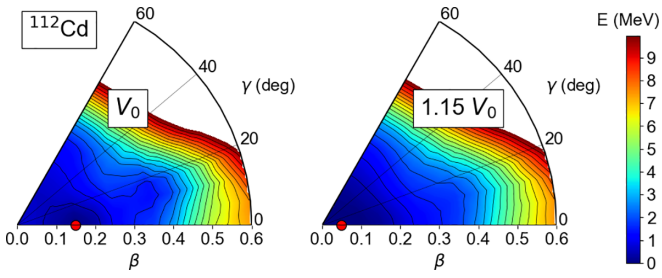

FIG. 3. Potential energy surfaces for ^{112}Cd obtained from the constrained RHB method, with the pairing strength unchanged "V_0" (left) and increased by 15% for both protons and neutrons "1.15V_0" (right).

Figure 5 compares the excitation energies for ^{112}Cd, obtained with the pairing strengths unchanged $(V_p, V_n) = (V_0, V_0)$, increased by 15% for protons only $(V_p, V_n) = (1.15V_0, V_0)$, for neutrons only $(V_p, V_n) = (V_0, 1.15V_0)$, and for both protons and neutrons $(V_p, V_n) = (1.15V_0, 1.15V_0)$, in the RHB calculations. It is seen that the increase in the proton pairing does not have any notable effect on energy spectra, but enhances the $B(E2; 0_2^+ \to 2_1^+)$ and $\rho^2(E0; 0_2^+ \to 0_1^+)$ transition probabilities. On the other hand, if the neutron pairing strength is increased, the 0_2^+ level is raised to be closer in energy to the experimental counterpart. In this case, however, the whole energy spectrum becomes stretched, and overestimates the experimental spectrum. The finding that the change in the proton pairing strength does not have notable influence on the spectra reflects the fact that the studied Cd nucleus is close to the proton $Z = 50$ major shell closure, around which the number of valence protons ($Z_{\rm val} = 2$) is not large enough to make a sizable contribution to the low-energy spectra. On the other hand, the increase in the neutron pairing appears to have a more significant effect on the low-lying levels than that for the proton pairing. This is probably because, as the nucleus is close to the middle of the neutron major shell $N = 50$–82, there are more valence neutrons ($N_{\rm val} = 14$ for ^{112}Cd), which are supposed to play a more dominant role in low-lying states.

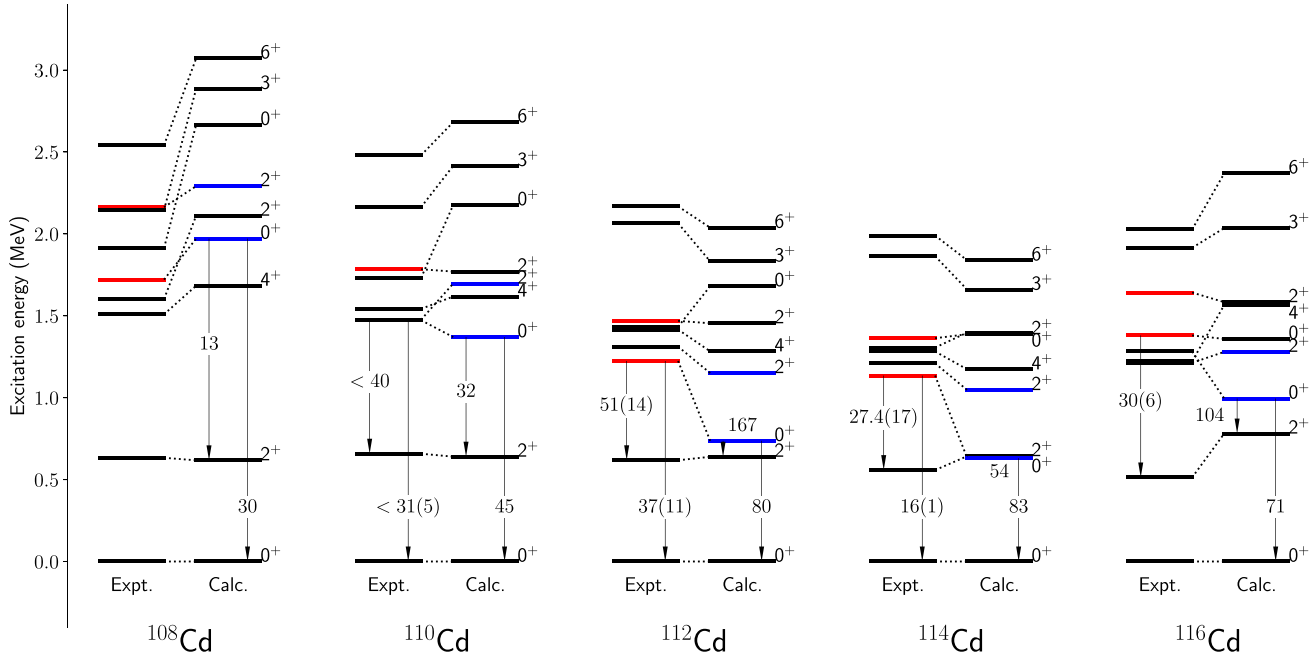

FIG. 4. Comparison between the calculated and experimental low-energy spectra for the even-even $^{108-116}$Cd isotopes. Numbers with arrows from the 0_2^+ level to 2_1^+ and 0_1^+ represent the $B(E2;0_2^+ \to 2_1^+)$ values in Weisskopf units (W.u.), and the $\rho^2(E0;0_2^+ \to 0_1^+) \times 10^3$ values, respectively. Only for ^{114}Cd, the calculated 0_2^+ level is below the 2_1^+ one, and therefore the $B(E2;2_1^+ \to 0_2^+)$ value is given. The experimental data are taken from Refs. [19,36,37,51,52]. The experimental levels that are highlighted in color red represent the suggested intruder states, while the corresponding theoretical levels are in color blue.

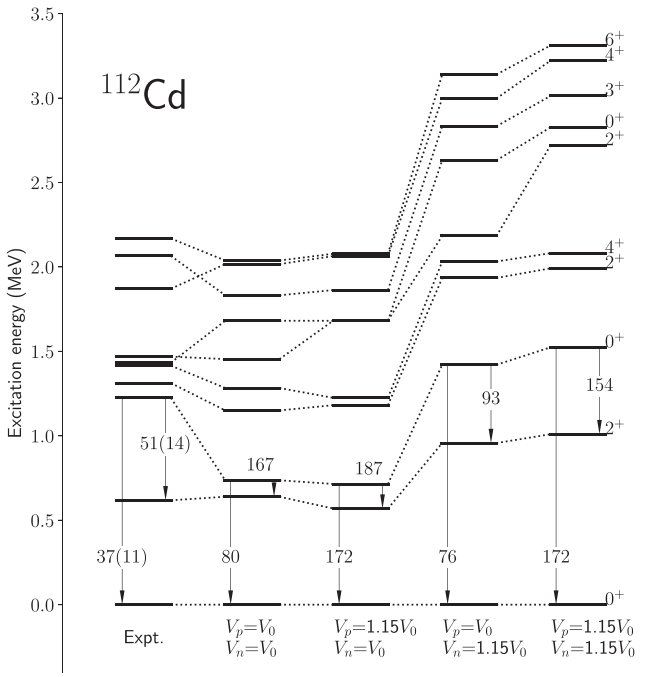

FIG. 5. Predicted excitation spectra for ^{112}Cd with the pairing strength unchanged ($V_p = V_0, V_n = V_0$), increased by 15% for protons only ($V_p = 1.15V_0$, $V_n = V_0$), for neutrons only ($V_p = V_0$, $V_n = 1.15V_0$), and for both protons and neutrons ($V_p = 1.15V_0$, $V_n = 1.15V_0$) in the RHB calculations. $B(E2;0_2^+ \to 2_1^+)$ (in W.u.) and $\rho^2(E0;0_2^+ \to 0_1^+) \times 10^3$ values are also shown. The experimental data are taken from [36].

Furthermore, the fact that increasing the pairing strength generally raises the energy levels, as one observes in Fig. 5, is also anticipated from the comparison of the potential energy surfaces (see Fig. 3), which have been obtained with the pairing strength increased and unchanged in the constrained RHB calculations. With the increased pairing, the energy surface indicates a less deformed shape; hence the energy spectrum should become more of vibrational character.

To provide an insight into the intruder nature of the predicted excited states, in Fig. 6 we show the distributions of the collective wave functions in the β-γ plane for the $0_{1,2,3}^+$ and $2_{1,2,3}^+$ states of $^{108-116}$Cd. The wave function of the 0_1^+ ground state in all the studied nuclei is sharply peaked at weakly deformed (triaxial) configurations $(\beta, \gamma) \approx (0.15, 20°–40°)$, the coordinate corresponding to the weakly deformed global minimum in the potential energy surface (see Fig. 1). The 0_2^+ wave function shows a sharp peak at larger deformation, $(\beta, \gamma) \approx (0.35, 10°)$. This deformation configuration corresponds to the local minimum near the prolate axis in the potential energy surfaces; hence the 0_2^+ is here assigned to be the bandhead of the intruder band. Two major peaks are obtained for the 0_2^+ wave function for ^{116}Cd: $(\beta, \gamma) \approx (0.35, 15°)$ and $(0.1, 30°)$. The one at $(\beta, \gamma) \approx (0.35, 15°)$ is also spread along the γ deformation. Hence, a considerable amount of shape mixing is expected to be present in the 0_2^+ state of ^{116}Cd. This is related to the fact that the energy surface for ^{116}Cd is considerably soft in the γ direction.

The 0_3^+ wave function distributions, shown in the third row of Fig. 6, generally exhibit a major peak on the oblate side, corresponding to the local oblate minimum or saddle

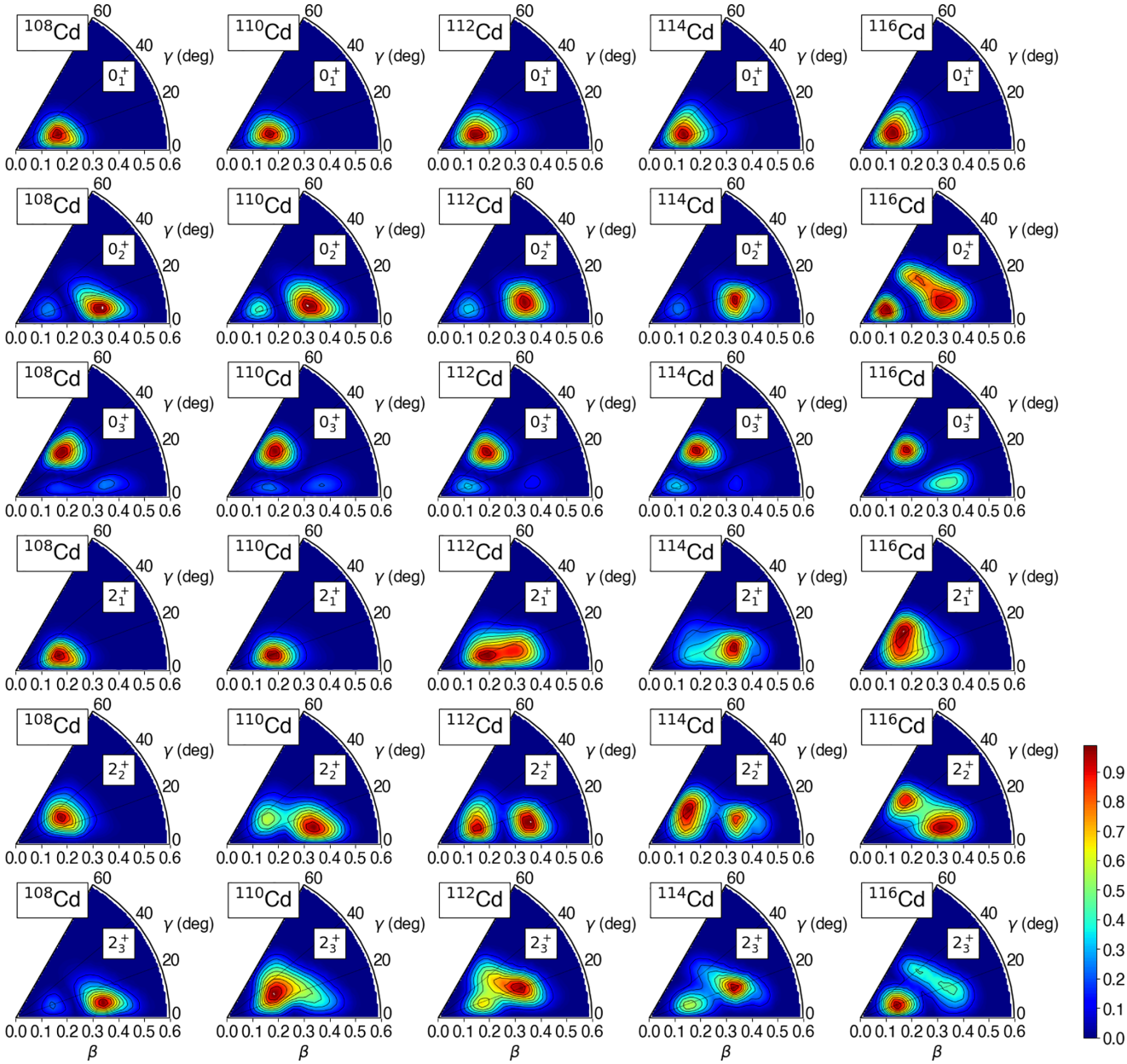

FIG. 6. Distributions of collective wave functions for the $0^+_{1,2,3}$, and $2^+_{1,2,3}$ states of $^{108-116}$Cd within the (β, γ) plane.

point. The 2^+_1 collective wave function for $^{108-112}$Cd shows a similar distribution pattern to 0^+_1, as it is peaked at $(\beta, \gamma) \approx (0.15, 20^\circ)$. For the 2^+_1 states of ^{114,116}Cd, however, the peak appears at $(\beta, \gamma) \approx (0.35, 15^\circ)$ for ^{114}Cd and $(0.2, 40^\circ)$ for ^{116}Cd, at variance with the distribution patterns of the respective 0^+_1 collective wave functions. The 2^+_1 wave function for $^{112-116}$Cd is also spread over wider regions in the (β, γ) plane than for ^{108,110}Cd. This implies that the mixing between different shape configurations is present already in the normal state 2^+_1 of $^{112-116}$Cd. The calculated 2^+_2 states for $^{110-116}$Cd, and 2^+_3 state for ^{108}Cd, can be associated with the 2^+ members of the observed intruder states, based on the fact that in the present calculation these nonyrast 2^+ states are shown to exhibit a particularly strong $E2$ transition to the 0^+_2 state (see Fig. 4). Indeed, for most of these nuclei, the collective wave function distribution gives two peaks, which have a large overlap with the 0^+_2 wave function. Furthermore, the calculation suggests the 2^+_3 (2^+_2) state for $^{110-116}$Cd (^{108}Cd) to be the bandhead of the lowest γ-vibrational or $K = 2^+$ band. This interpretation is based on the dominance of the $K = 2$ components in these states. The corresponding collective wave functions are indeed peaked at the triaxial region with $\gamma \approx 30^\circ$. Figure 7 shows the calculated low-energy band structure including $B(E2)$ transition probabilities for ^{110}Cd, in comparison with the experimental data [36]. For the theoretical energy spectra, states are classified into the ground-state, lowest three $K = 0^+$, and lowest two $K = 2^+$ bands according to the dominant $E2$ transitions within the

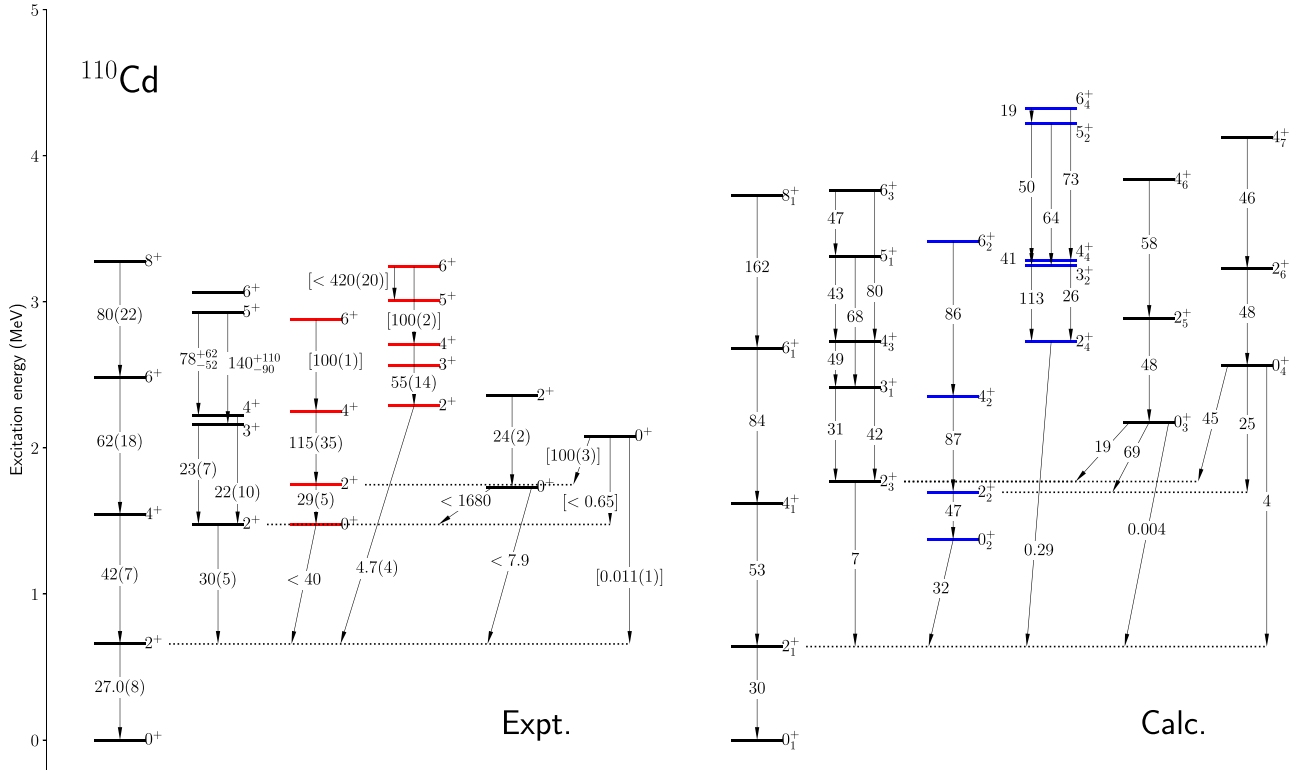

FIG. 7. Calculated and experimental [36] excitation spectra and $B(E2)$ transition rates (in W.u.) for the ^{110}Cd nucleus. Following the notations in Ref. [36], the experimental $B(E2)$ values in parentheses stand for relative transition strengths. The experimental levels that are highlighted in color red represent the suggested intruder states, and the corresponding theoretical levels are in color blue.

band and to the similarity in the fractions of the $K = 0$, 2, and 4 components. The observed low-energy spectra have multiphonon structure typical of vibrational nuclei, that is, the approximate one-phonon state 2_1^+, two-phonon triplet (4_1^+, 2_2^+, 0_3^+) at twice its energy, and three-phonon quintet (6_1^+, 4_2^+, 3_1^+, 2_5^+, 0_4^+) at three times the 2_1^+ energy. The $\Delta I = 2$ band built on the excited 0_2^+ state has been assigned to be an intruder band by experiment [36]. The second $K = 2^+$ band, which is based upon the 2_4^+ state, has also been found to be the intruder γ band experimentally. In the present calculation, a phonon-like level structure appears as the closely lying (4_1^+, 2_3^+, 0_3^+) and (6_1^+, 4_3^+, 3_1^+, 2_5^+, 0_4^+) states. The intruder bands that can be identified by the RHB+QCH calculation are those based on the 0_2^+ and 2_4^+ states. The calculation reproduces the $K = 0_2^+$ intruder band rather well, except that the the energy level of the 6^+ member is overestimated. A large transition strength $B(E2; 0_2^+ \to 2_1^+) = 32$ W.u. is here obtained, being consistent with the experimental value <40 W.u. The intruder γ (or second $K = 2^+$) band is, however, calculated to be rather high and stretched in energy by the RHB+QCH, as compared with the data. States in the calculated second $K = 2^+$ band are connected by the strong $\Delta I = 1$, as well as $\Delta I = 2$, in-band $E2$ transitions. The calculated $K = 0_3^+$ (0_4^+) band is slightly higher than the observed one, and exhibits large interband $E2$ transition probabilities $B(E2; 0^+_{K=0_3^+} \to 2^+_{K=2^+}) = 19$ W.u. and $B(E2; 0^+_{K=0_3^+} \to 2^+_{K=0_2^+}) = 69$ W.u. [$B(E2; 0^+_{K=0_4^+} \to 2^+_{K=2^+}) = 45$ W.u. and $B(E2; 0^+_{K=0_4^+} \to 2^+_{K=0_2^+}) = 25$ W.u.]. Here $2^+_{K=2^+}$ and $2^+_{K=0_2^+}$ denote the 2_3^+ bandhead of the lowest $K = 2^+$ and the 2^+ member of the $K = 0_2^+$ band, respectively. The spectroscopic quadrupole moment for the 2_1^+ state is calculated to be $Q(2_1^+) = -0.53$ e b, slightly larger in magnitude than the experimental value $-0.40(3)$ e b [36].

Figure 8 shows the energy spectra for ^{112}Cd. The whole energy spectrum, both theoretical and experimental, appears to be rather compressed in comparison with ^{110}Cd. The present RHB+QCH calculation reproduces the observed energy levels reasonably well, apart from the fact that the 0_2^+ band is obtained at much lower energy and is more stretched with increasing spin than in experiment. Similarly to the case of ^{110}Cd, in addition to the phonon-like states grouped into approximate multiplets (4_1^+, 2_2^+, 0_3^+), (6_1^+, 4_3^+, 3_1^+, 2_4^+, 0_4^+), …, etc., the states belonging to the band built on the 0_2^+ state, together with the additional 2_6^+ and 3_2^+ states, have been experimentally suggested to be intruder states arising from the proton 2p-2h excitations. The corresponding two intruder bands in the present calculation are the ones starting from the 0_2^+ and 2_4^+ states. A possible reason for the $K = 0_2^+$ band being calculated to be significantly low in energy is that the local triaxial minimum at $(\beta, \gamma) \approx (0.35, 12^\circ)$ in the potential energy surface is too pronounced (see Fig. 1). The states belonging to the 0_2^+ band are mainly constructed from this local minimum. The fact that the calculated transition rate $B(E2; 0_2^+ \to 2_1^+) = 167$ W.u. is a factor of three greater than the measured one (51 ± 14 W.u.) further corroborates the occurrence of strong shape mixing. The predicted 0_3^+ and 0_4^+ excitation energies are, however, close to the experimental

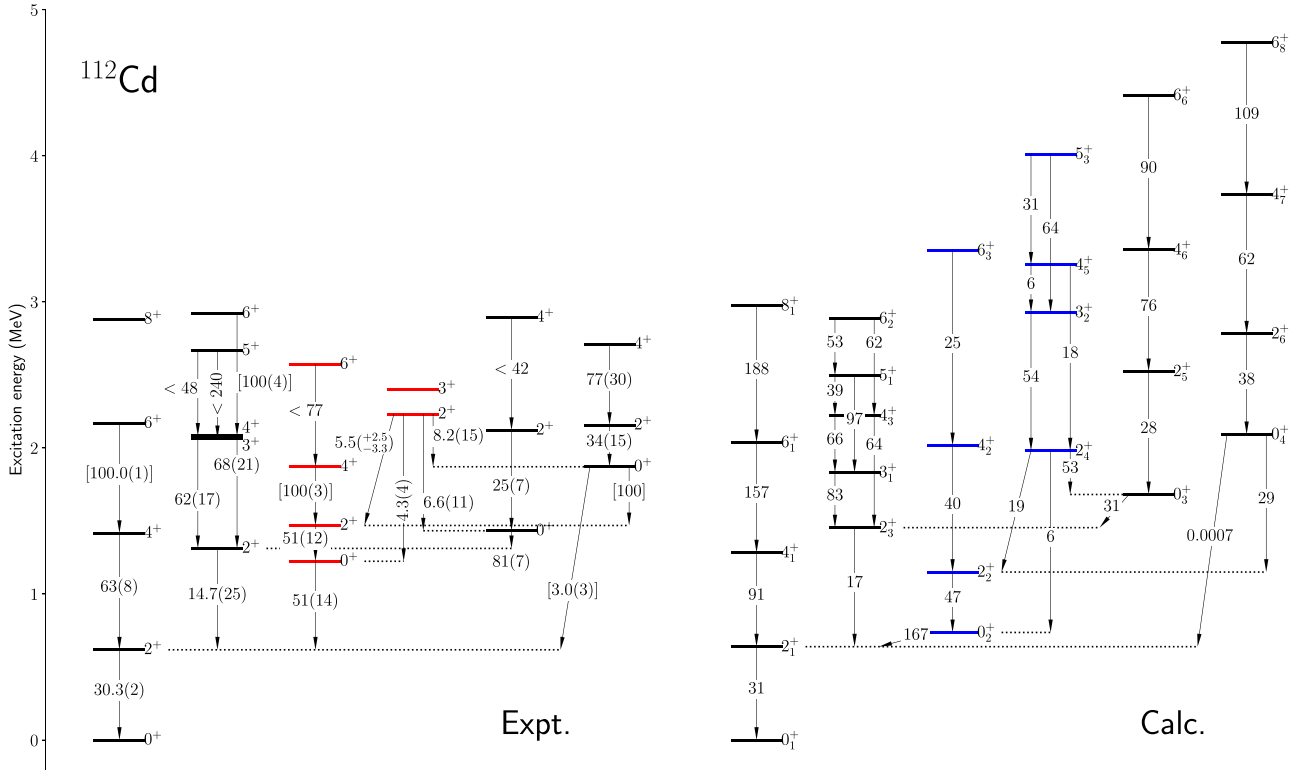

FIG. 8. Same as Fig. 7, but for the ^{112}Cd nucleus.

ones. Their $E2$ selection rules also follow what are observed experimentally: the large transition probability from the 0_3^+ state to the $2^+_{K=2^+}$ bandhead [$B(E2;0_3^+ \to 2_3^+) = 31$ W.u.] and the dominance of the $0^+_{K=0_4^+} \to 2^+_{K=0_2^+}$ $E2$ transition over the $0^+_{K=0_4^+} \to 2^+_{\rm gs}$ one. The $Q(2_1^+)$ moment of ^{112}Cd is calculated to be -0.68 e b, which is larger in magnitude than the experimental value $Q(2_1^+) = -0.38$ e b [36], as in the ^{110}Cd case discussed earlier.

Recent theoretical calculations for ^{110,112}Cd [36,37] within the symmetry conserving configuration mixing (SCCM) method using the Gogny force generally overestimated the energy levels of the observed excited 0^+ states, whereas in the present RHB+QCH calculation these 0^+ energy levels, particularly the one for the second 0^+ state, are predicted to be much lower. In addition, the same Gogny plus SCCM calculations provided the ground-state band for both the ^{110,112}Cd nuclei that is rather stretched in energy with respect to the one obtained in the present calculation. It should be noted that, in solving the collective Hamiltonian in the present study, we do not make any adjustment of the cranking moment of inertia, e.g., increase of it by 30%–40% to reproduce experiment, that is often considered in the literature.

The IBM calculation, using the boson Hamiltonian with partial dynamical symmetry (PDS) breaking [32] and taking into account the configuration mixing between normal and intruder states, was also carried out to study the possible breakdown of the vibrational structure of ^{110}Cd. By virtue of introducing the PDS, the IBM calculation obtained additional low-lying states close in energy to the normal vibrational states, which correspond to the empirically suggested intruder states. The calculated energy spectra and $B(E2)$ rates reported in that reference fit very well the experimental ones, while the parameters for the boson Hamiltonian and effective charges for the quadrupole operator were there determined by a phenomenological adjustment to the empirical data.

V. SUMMARY

In summary, we have analyzed the structure of the even-even $^{108-116}$Cd isotopes within the framework of a general collective model that is based on the nuclear density functional theory. Parameters of the triaxial quadrupole collective Hamiltonian, i.e., deformation-dependent mass parameters, moments of inertia, and collective potential, are determined by using as microscopic inputs the solutions to the constrained mean-field calculations within the relativistic Hartree-Bogoliubov approach. The mean-field results for the near midshell nuclei ^{112,114}Cd indicate coexistence of normal states that are associated with a weakly deformed prolate or nearly spherical global minimum, and intruder states constructed from a more deformed, nearly prolate triaxial, local minimum.

Observed low-energy spectra, $B(E2)$, and $\rho^2(E0)$ values have been described reasonably well by the collective Hamiltonian. The present spectroscopic calculation produced a low-energy 0_2^+ band and an additional γ-vibrational band which correspond to a triaxial local minimum in the potential

energy surface, consistent with the empirical assignment of these bands as intruder bands. The calculation has reproduced an observed decrease of the intruder bands toward the midshell $N = 66$ as a function of nucleon number. The intruder interpretation of the 0_2^+ band associated with the local minimum has been further confirmed by distributions of the collective wave functions in the β-γ plane. For ^{112,114}Cd, however, the QCH underestimates the observed intruder bands significantly, and results in the too large $B(E2; 0_2^+ \to 2_1^+)$ and $\rho^2(E0; 0_2^+ \to 0_1^+)$ values, even though the approximate multiplets of energy levels typical of the phonon-like normal states were reasonably described. The discrepancy in the intruder bands reflects the too pronounced triaxial local minimum, which reflects, to a large extent, properties of the energy density functional employed in this study. We have also studied the sensitivity of the results to the pairing strengths in the case of ^{112}Cd. It has been shown that with the increase in the strength of the (especially neutron) pairing, the local minima disappear in the potential energy surface, leading to a less deformed structure, and the corresponding energy levels are significantly raised.

ACKNOWLEDGMENTS

The authors are grateful to Antonio Bjelčić for helping them with implementation of the modified RHB solver. This work is financed within the Tenure Track Pilot Programme of the Croatian Science Foundation and the École Polytechnique Fédérale de Lausanne, and the Project TTP-2018-07-3554 Exotic Nuclear Structure and Dynamics, with funds of the Croatian-Swiss Research Programme.

[1] A. Bohr and B. R. Mottelson, *Nuclear Structure* (Benjamin, New York, 1975), Vol. II.
[2] P. Ring and P. Schuck, *The Nuclear Many-Body Problem* (Springer-Verlag, Berlin, 1980).
[3] R. F. Casten, *Nuclear Structure from a Simple Perspective* (Oxford University Press, Oxford, 2000).
[4] F. Iachello and A. Arima, *The Interacting Boson Model* (Cambridge University Press, Cambridge, 1987).
[5] G. Scharff-Goldhaber and J. Weneser, Phys. Rev. **98**, 212 (1955).
[6] B. L. Cohen and R. E. Price, Phys. Rev. **121**, 1441 (1961).
[7] P. Federman and S. Pittel, Phys. Lett. B **69**, 385 (1977).
[8] K. Heyde, P. Van Isacker, R. F. Casten, and J. L. Wood, Phys. Lett. B **155**, 303 (1985).
[9] K. Heyde, C. De Coster, J. Jolie, and J. L. Wood, Phys. Rev. C **46**, 541 (1992).
[10] J. L. Wood, K. Heyde, W. Nazarewicz, M. Huyse, and P. van Duppen, Phys. Rep. **215**, 101 (1992).
[11] K. Heyde, J. Jolie, H. Lehmann, C. De Coster, and J. Wood, Nucl. Phys. A **586**, 1 (1995).
[12] K. Heyde and J. L. Wood, Rev. Mod. Phys. **83**, 1467 (2011).
[13] H. Fielding, R. Anderson, C. Zafiratos, D. Lind, F. Cecil, H. Wieman, and W. Alford, Nucl. Phys. A **281**, 389 (1977).
[14] R. Bengtsson, T. Bengtsson, J. Dudek, G. Leander, W. Nazarewicz, and J. Zhang, Phys. Lett. B **183**, 1 (1987).
[15] R. Bengtsson and W. Nazarewicz, Z. Phys. A **334**, 269 (1989).
[16] A. N. Andreyev, M. Huyse, P. Van Duppen, L. Weissman, D. Ackermann, J. Gerl, F. P. Hessberger, S. Hofmann, A. Kleinböhl, G. Münzenberg, S. Reshitko, C. Schlegel, H. Schaffner, P. Cagarda, M. Matos, S. Saro, A. Keenan, C. Moore, C. D. O'Leary, R. D. Page *et al.*, Nature (London) **405**, 430 (2000).
[17] K. Nomura and J. Jolie, Phys. Rev. C **98**, 024303 (2018).
[18] P. E. Garrett and J. L. Wood, J. Phys. G: Nucl. Part. Phys. **37**, 064028 (2010).
[19] P. E. Garrett, J. Phys. G: Nucl. Part. Phys. **43**, 084002 (2016).
[20] P. E. Garrett, M. Zieliska, and E. Clément, Prog. Part. Nucl. Phys. **124**, 103931 (2022).
[21] M. Górska, M. Lipoglavšek, H. Grawe, J. Nyberg, A. Atac, A. Axelsson, R. Bark, J. Blomqvist, J. Cederkäll, B. Cederwall, G. de Angelis, C. Fahlander, A. Johnson, S. Leoni, A. Likar, M. Matiuzzi, S. Mitarai, L.-O. Norlin, M. Palacz, J. Persson *et al.*, Phys. Rev. Lett. **79**, 2415 (1997).
[22] A. Blazhev, M. Górska, H. Grawe, J. Nyberg, M. Palacz, E. Caurier, O. Dorvaux, A. Gadea, F. Nowacki, C. Andreoiu, G. de Angelis, D. Balabanski, C. Beck, B. Cederwall, D. Curien, J. Döring, J. Ekman, C. Fahlander, K. Lagergren, J. Ljungvall *et al.*, Phys. Rev. C **69**, 064304 (2004).
[23] A. Ekström, J. Cederkäll, D. D. DiJulio, C. Fahlander, M. Hjorth-Jensen, A. Blazhev, B. Bruyneel, P. A. Butler, T. Davinson, J. Eberth, C. Fransen, K. Geibel, H. Hess, O. Ivanov, J. Iwanicki, O. Kester, J. Kownacki, U. Köster, B. A. Marsh, P. Reiter *et al.*, Phys. Rev. C **80**, 054302 (2009).
[24] T. Schmidt, K. L. G. Heyde, A. Blazhev, and J. Jolie, Phys. Rev. C **96**, 014302 (2017).
[25] K. Heyde, P. Van Isacker, M. Waroquier, G. Wenes, and M. Sambataro, Phys. Rev. C **25**, 3160 (1982).
[26] M. Délèze, S. Drissi, J. Kern, P. Tercier, J. Vorlet, J. Rikovska, T. Otsuka, S. Judge, and A. Williams, Nucl. Phys. A **551**, 269 (1993).
[27] M. Délèze, S. Drissi, J. Jolie, J. Kern, and J. Vorlet, Nucl. Phys. A **554**, 1 (1993).
[28] C. De Coster, K. Heyde, B. Decroix, P. Van Isacker, J. Jolie, H. Lehmann, and J. L. Wood, Nucl. Phys. A **600**, 251 (1996).
[29] H. Lehmann, J. Jolie, C. De Coster, B. Decroix, K. Heyde, and J. L. Wood, Nucl. Phys. A **621**, 767 (1997).
[30] P. E. Garrett, K. L. Green, H. Lehmann, J. Jolie, C. A. McGrath, M. Yeh, and S. W. Yates, Phys. Rev. C **75**, 054310 (2007).
[31] P. E. Garrett, K. L. Green, and J. L. Wood, Phys. Rev. C **78**, 044307 (2008).
[32] A. Leviatan, N. Gavrielov, J. E. García-Ramos, and P. Van Isacker, Phys. Rev. C **98**, 031302(R) (2018).
[33] J. Decharge, M. Girod, and D. Gogny, Phys. Lett. B **55**, 361 (1975).
[34] J. F. Berger, M. Girod, and D. Gogny, Nucl. Phys. A **428**, 23 (1984).
[35] T. R. Rodríguez, J. L. Egido, and A. Jungclaus, Phys. Lett. B **668**, 410 (2008).
[36] P. E. Garrett, T. R. Rodríguez, A. D. Varela, K. L. Green, J. Bangay, A. Finlay, R. A. E. Austin, G. C. Ball, D. S.

Bandyopadhyay, V. Bildstein, S. Colosimo, D. S. Cross, G. A. Demand, P. Finlay, A. B. Garnsworthy, G. F. Grinyer, G. Hackman, B. Jigmeddorj, J. Jolie, W. D. Kulp *et al.*, Phys. Rev. Lett. **123**, 142502 (2019).

[37] P. E. Garrett, T. R. Rodríguez, A. Diaz Varela, K. L. Green, J. Bangay, A. Finlay, R. A. E. Austin, G. C. Ball, D. S. Bandyopadhyay, V. Bildstein, S. Colosimo, D. S. Cross, G. A. Demand, P. Finlay, A. B. Garnsworthy, G. F. Grinyer, G. Hackman, B. Jigmeddorj, J. Jolie, W. D. Kulp *et al.*, Phys. Rev. C **101**, 044302 (2020).

[38] M. Siciliano, J. J. Valiente-Dobón, A. Goasduff, T. R. Rodríguez, D. Bazzacco, G. Benzoni, T. Braunroth, N. Cieplicka-Oryńczak, E. Clément, F. C. L. Crespi, G. de France, M. Doncel, S. Ertürk, C. Fransen, A. Gadea, G. Georgiev, A. Goldkuhle, U. Jakobsson, G. Jaworski, P. R. John *et al.*, Phys. Rev. C **104**, 034320 (2021).

[39] T. H. R. Skyrme, Nucl. Phys. **9**, 615 (1958).

[40] L. Próchniak, P. Quentin, and M. Imadalou, Int. J. Mod. Phys. E **21**, 1250036 (2012).

[41] D. Vretenar, A. V. Afanasjev, G. A. Lalazissis, and P. Ring, Phys. Rep. **409**, 101 (2005).

[42] T. Nikšić, D. Vretenar, and P. Ring, Prog. Part. Nucl. Phys. **66**, 519 (2011).

[43] T. Nikšić, N. Paar, D. Vretenar, and P. Ring, Comput. Phys. Commun. **185**, 1808 (2014).

[44] A. Bjelčić, T. Nikšić, and Z. Drmač, DIRHBspeedup, https://github.com/abjelcic/DIRHBspeedup.git (2021).

[45] T. Nikšić, D. Vretenar, and P. Ring, Phys. Rev. C **78**, 034318 (2008).

[46] Y. Tian, Z. Y. Ma, and P. Ring, Phys. Lett. B **676**, 44 (2009).

[47] T. Nikšić, Z. P. Li, D. Vretenar, L. Próchniak, J. Meng, and P. Ring, Phys. Rev. C **79**, 034303 (2009).

[48] D. R. Inglis, Phys. Rev. **103**, 1786 (1956).

[49] S. Beliaev, Nucl. Phys. **24**, 322 (1961).

[50] E. Chabanat, P. Bonche, P. Haensel, J. Meyer, and R. Schaeffer, Nucl. Phys. A **635**, 231 (1998).

[51] T. Kibédi and R. Spear, At. Data Nucl. Data Tables **89**, 77 (2005).

[52] Brookhaven National Nuclear Data Center, https://www.nndc.bnl.gov.

[53] A. Gade, J. Jolie, and P. von Brentano, Phys. Rev. C **65**, 041305(R) (2002).